IOP Publishing Journal of Physics D: Applied Physics

J. Phys. D: Appl. Phys. **49** (2016) 405104 (6pp) doi:10.1088/0022-3727/49/40/405104

Direct and indirect coupling mechanisms in a chiral plasmonic system

Yongkai Wang, Xiaojing Wen, Yu Qu, Tong Fu and Zhongyue Zhang

School of Physics and Information Technology, Shaanxi Normal University, Xi'an 710062, People's Republic of China

E-mail: zyzhang@snnu.edu.cn

Received 28 July 2016, revised 14 August 2016
Accepted for publication 22 August 2016
Published 13 September 2016

Abstract

Artificial chiral plasmonic nanostructures (ACPNs) are widely studied and used in biological monitoring, analytical chemistry, and negative-refractive-index media. The mechanism of direct coupling between two twist metal nanorods has been obtained in usual ACPNs. In this work, we proposed a nanosystem of twist nanorods separated by a metal film (TNMF). By analyzing the charge distributions, a new indirect coupling mechanism is found. According to the equivalent *LC* resonant circuits, gold nanorods on the two sides of the gold film can be regarded as a receiver and an emitter. These components enhanced transmittance and provided direct and indirect coupling mechanisms for the circular dichroism (CD). The direct coupling mode cannot be explained by impedance matching and can be tuned monotonously by monotonously varying geometric dimensions. However, the CD signal of indirect coupling can be explained by impedance matching and can be tuned to its maximum by varying geometric dimensions when the impedances of both sides of the gold film match. These results can help design novel chiral optical structures and promote combined applications between photons and electrons when a gold film is powered on.

Keywords: circular dichroism, surface plasmon polariton, plasmonics, resonance

(Some figures may appear in colour only in the online journal)

1. Introduction

Chiral nanostructures cannot be made to coincide with their mirror images In 1969, Sherman demonstrated the optical property of chiral chlorophyll-a, which presents different optical responses to right circularly polarized (RCP, +) and left circularly polarized (LCP, −) light [1], i.e. circular dichroism (CD) [2–4]. Considering the strong interaction between light with noble metals, artificial chiral plasmonic nanostructures (ACPNs) show stronger CD than chiral biomolecules [5, 6]. The mechanism of generating CD is due to the coupling of electric and magnetic dipole moments [7]. ACPNs are widely applied in biological monitoring [8–10], analytical chemistry [11–13], broadband circular polarization [3, 14], and negative refractive-index media [15–17].

Recently, researchers have proposed different ACPNs to explore the mechanism of chirality and produce strong chiral signal. Two-dimensional (2D) achiral plasmonic nanoparticles under obliquely excitation and 2D chiral plasmonic nanoparticles under normally excitation can all achieve CD signal. Three-dimensional (3D) ACPNs show stronger chirality than 2D ACPNs, such as helices [18–20] or L-shaped ACPNs in our previous work [21]. Given the simple fabrication of layer-by-layer 3D ACPNs [22, 23], they are attracting increased research interest. Layer-by-layer ACPNs also achieve a stronger CD signal than single-layer ones [24–26] because of direct electromagnetic coupling between two layers [23]. In the above-mentioned ACPNs, direct coupling between electron oscillations results in CD effect. When a metal film is used to separate two electric dipole moments, interesting optical properties and novel coupling arise.

In this paper, we proposed twist nanorods separated by metal film (TNMF), and its CD effect was investigated by finite-element method. Except for direct coupling mechanism between electric dipole moments on two nanorods, a new indirect coupling mechanism is found and also leads to CD effects. The mechanism of direct coupling is similar to that of twist nanorods [27]. For indirect coupling

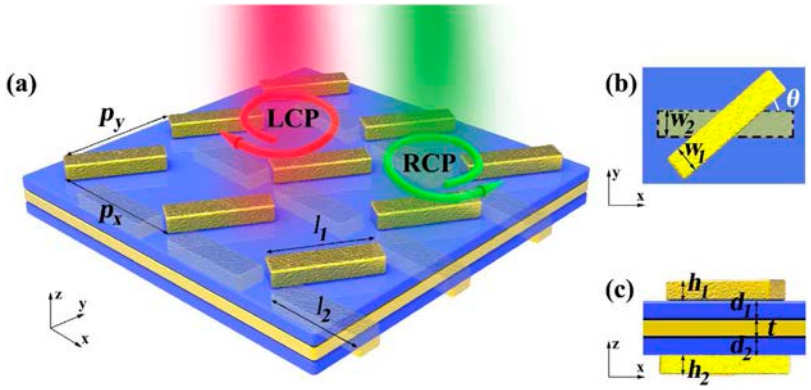

Figure 1. Schematic of (a) TNMF arrays and parameters definition, where the unit cell with the associated geometric features is designated in (b) *x*-*y* plane and (c) *x*-*z* plane.

mechanism, nanorods at the incident side of the film and nanorods at the outgoing side of the film can be regarded as absorber and emitter, respectively [28, 29]. Only when impedances of absorbers and emitter match does the maximum CD appears in indirect coupling, which is very special property relative to direct coupling. The effects of other geometric dimensions on CD effect were also studied and proved the different properties between direct and indirect coupling mechanisms.

2. Structure and computational method

Figure 1(a) shows the proposed TNMF arrays, where a pair of periodic and twist gold nanorods (yellow) are separated by a continuous gold film (yellow). SiO_2 layers (blue) are placed between nanorods and gold film. The periods in x and y direction are fixed with $p_x = 200\,\text{nm}$ and $p_y = 200\,\text{nm}$, respectively. The lengths of top and bottom nanorods are labeled as l_1 and l_2, respectively. Figure 1(b) shows the cell of TNMF in x-y plane. The bottom nanorod is presented in magenta dash line. θ is the twist angle between two nanorods in x-y plane. w_1 and w_2 are widths of top and bottom nanorods, respectively. Figure 1(c) shows the cell of TNMF in x-z plane. h_1 and h_2 are the heights of top and bottom nanorods, respectively. d_1 and d_2 are the thicknesses of top and bottom SiO_2 layers, respectively. t is the thickness of gold film. In this study, we select a control group for TNMF arrays with $l_1 = l_2 = 80\,\text{nm}$, $w_1 = w_2 = 20\,\text{nm}$, $h_1 = h_2 = 20\,\text{nm}$, $d_1 = d_2 = 30\,\text{nm}$, $\theta = 45°$, and $t = 30\,\text{nm}$.

The 3D finite-element method software COMSOL Multiphysics is used to calculate the transmittance of TNMF arrays. The refractive index of gold is taken from [30], and the refractive index of SiO_2 is 1.45. The excitation sources are RCP light and LCP light along the $-z$-direction and the magnitude of the incident electric field is set at $1\,\text{V m}^{-1}$. The infinite array is simulated using unit cell with periodic boundary conditions along the x and y directions. The transmittance is defined as $T = P_{\text{out}}/P_{\text{in}}$, which is the ratio of output power to incident power. The transmittance spectrum of RCP light and LCP light are represented by T_{++} and T_{--}, respectively. Therefore, the chirality of TNMF arrays is represented by $\text{CD} = T_{++} - T_{--}$.

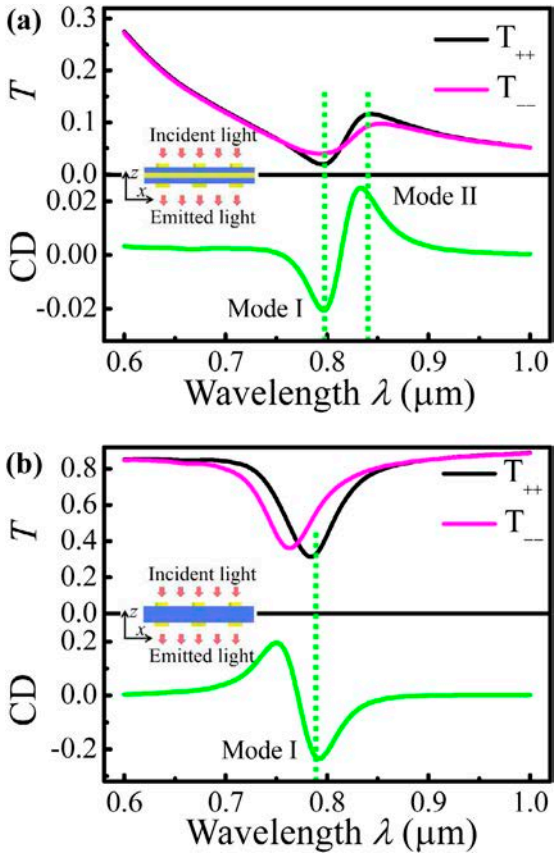

Figure 2. Simulated T_{++}, T_{--}, and CD spectra of (a) TNMF arrays and (b) TNGF arrays. Insets are the schematic of TNMF arrays and TNGF arrays in the view of x-z plane.

3. Result and discussion

Figure 2(a) shows T_{++} and T_{--} of TNMF arrays with the parameters of the control group. The wavelength ranges from 0.6 μm to 1.0 μm. The transmittance valleys and peaks of T_{++} and T_{--} occur around 0.80 and 0.84 μm, respectively. The transmittance differences at valleys and peaks lead to strong CD around 0.80 and 0.84 μm. For comparison, we calculate the transmittance spectra of twist nanorods arrays separated by glass layers (TNGF). The thickness of SiO_2 layers is the sum of d_1, d_2, and t in figure 1(c). Figure 2(b) shows that transmittance valleys occur at 0.760 and 0.780 μm for T_{++}

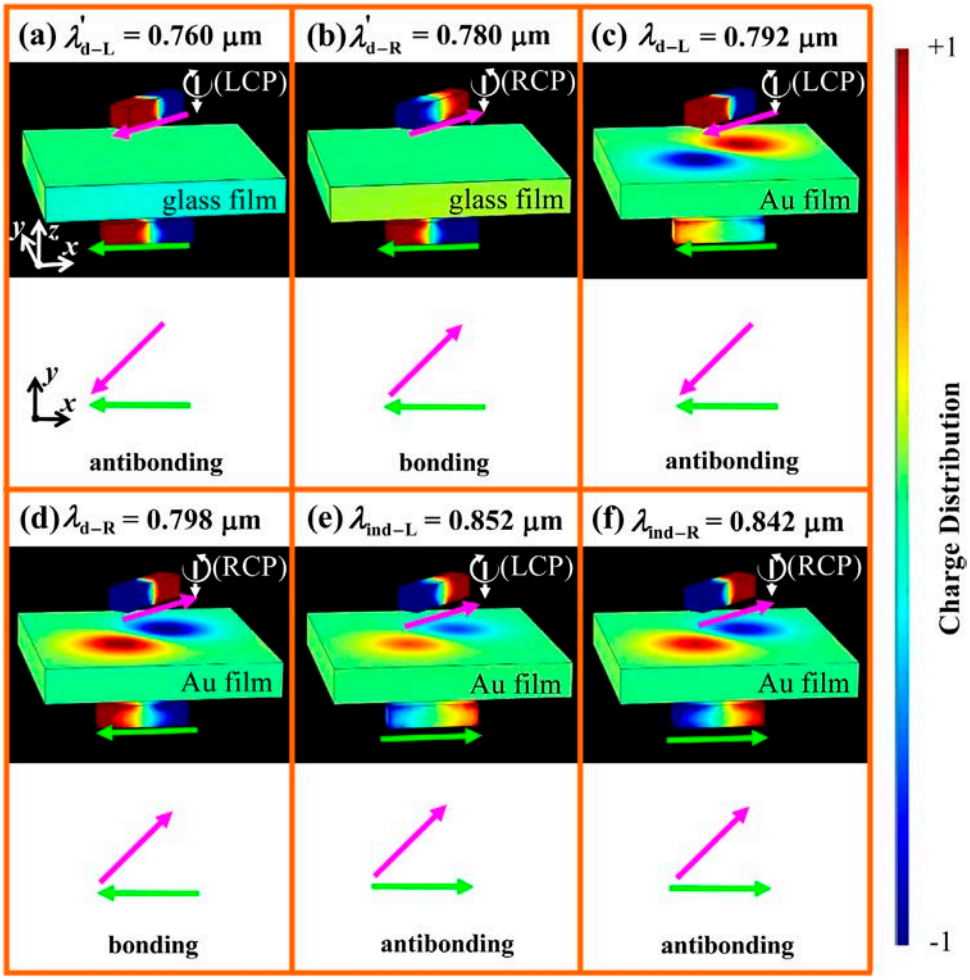

Figure 3. The charge distributions (color distributions) and Born–Kuhn modes (magenta and viridity arrows) at resonant wavelength for (a) and (b) TNGF arrays and (c)–(f) TNMF arrays. The resonances are labeled mode I and II.

and T_{--}, respectively. The transmittance difference at valleys leads to a strong CD effect.

To illustrate the mechanisms of CD effect, the normalized charge distributions at these resonant wavelengths in figure 2 are calculated. Figures 3(a) and (b) show twist nanorod arrays separated by SiO_2 layers, and figures 3(c)–(f) are for TNMF arrays. Red indicates positive a charge, and blue indicates a negative charge. The main charges are distributed on the two ends of every nanorod. The magenta and viridity arrows represent the equivalent electric dipole moments of top and bottom nanorods, respectively. The characteristic of charge distributions can show the coupling mode between nanorods. According to Born–Kuhn oscillator, the mechanism of generating CD is explained by the bonding and antibonding modes in two identical nanorods displaced vertically [27]. For right-handed ACPNs, bonding mode is more easily excited by LCP than by RCP light, which leads to a negative CD signal [27].

For twist nanorod arrays separated by SiO_2 layers, at λ'_{d-L}= 0.760 μm the magenta arrow and viridity arrow are translated into the *x*-*y* plane and form an antibonding mode in the the Born–Kuhn oscillator model [27], as shown in figure 3(a). Similarly, the magenta arrow and viridity arrow show a bonding mode at λ'_{d-R}= 0.780 μm in figure 3(b). These

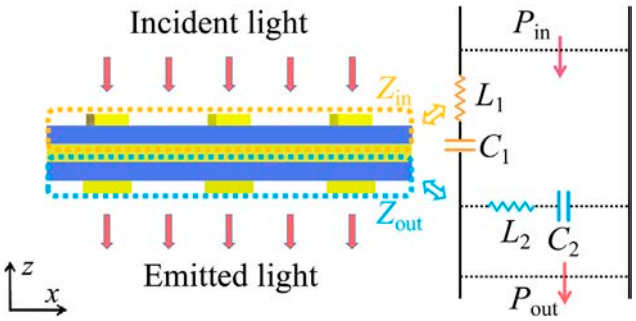

Figure 4. Schematic of TNMF arrays in *x*-*z* plane and schematic of equivalent transmission line.

two modes are similar to those of two twist nanorods in literature [27], and we call them direct coupling modes.

When SiO_2 layers are replaced by gold film in the middle layer (i.e. for TNMF arrays), new electric field coupling occurs. At λ_{d-L}= 0.792 μm, as shown in figure 3(c), the charge distribution at two nanorods is similar to that in figure 3(a). The electron oscillation on two nanorods also forms an antibonding mode. At λ_{d-R} = 0.798 μm, the magenta and viridity arrows form a bonding mode, as shown in figure 3(d), similar to that in figure 3(b) and belonging to direct coupling mode. As shown in figures 3(e) and (f), the charge distributions differ

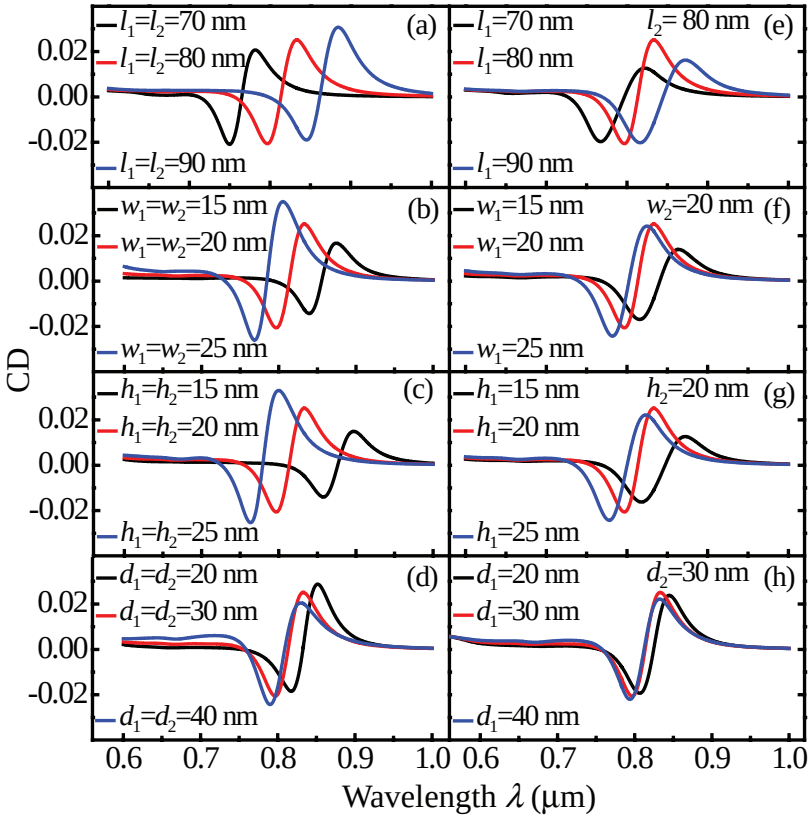

Figure 5. CD spectra of TNMF arrays with (a) different $l_1 = l_2$ values, (b) different $w_1 = w_2$ values, (c) different $h_1 = h_2$ values, (d) different $d_1 = d_2$ values, (e) different l_1 values with fixed $l_2 = 80$ nm, (f) different w_1 values with fixed $w_2 = 20$ nm, (g) different h_1 values with fixed $h_2 = 30$ nm, and (h) different d_1 values with fixed $d_2 = 30$ nm.

from those in figures 3(a) and (b). The electron oscillations show antibonding modes at $\lambda_{\mathrm{ind}-L} = 0.852\ \mu$m in figure 3(e) and $\lambda_{\mathrm{ind}-R} = 0.842\ \mu$m in figure 3(f). Given that the gold film changes in the coupling between nanorods, we call them indirect coupling modes.

Figure 4 shows that TNMF arrays can be decomposed as input and output parts, similar to a circuit system [31]. According to the equivalent *LC* resonant circuits, the resonant wavelength can be expressed as

$$\lambda_{LC} = 2\pi c\sqrt{LC},$$

where c is the speed of light in a vacuum, and L and C are the inductance and the capacitance of plasmonic nanostructures, respectively [28]. Figure 4 shows that TNMF arrays are separated into the input part circled by orange dash lines and the output part circled by blue dash lines in the x-y plane view. The former has an equivalent impedance Z_{in} (inductance L_{in} and capacitance C_{in}); the latter has an equivalent impedance Z_{out} (inductance L_{out} and capacitance C_{out}). Maximum transmission occurs when two resonance wavelengths equals each other, i.e. $Z_{\mathrm{in}} = Z_{\mathrm{out}}$.

For approximation, the inductance of straight metal wire with circular section is represented as

$$L \propto \frac{ul}{2\pi}\ln\frac{2l}{r},$$

where m, l, and r are the permeability of metal, the wire length, and the wire radius, respectively [32]. The equivalent radius for straight metal wire with rectangular section is obtained as

$$r = \sqrt{\frac{wh}{\pi}},$$

when $w \approx h$. The approximate inductance for the nanorod of input part can then be written as circular section is represented as

$$L_{\mathrm{in}} \propto \frac{l_1}{w_1 h_1}. \tag{1}$$

The capacitance between nanorod and metal surface is approximated as

$$C_{\mathrm{in}} \propto \frac{1}{d_1}, \tag{2}$$

The resonance wavelengths of the input and output parts are then represented respectively as

$$\lambda_{LC-\mathrm{in}} = 2\pi c\sqrt{L_{\mathrm{in}}C_{\mathrm{in}}} \propto \frac{l_1}{w_1 h_1 d_1}, \tag{3}$$

and

$$\lambda_{LC-\mathrm{out}} = 2\pi c\sqrt{L_{\mathrm{out}}C_{\mathrm{out}}} \propto \frac{l_2}{w_2 h_2 d_2}. \tag{4}$$

To analyze the effects of geometry parameters on direct and indirect coupling modes, we sequentially vary l, w, h, and d of TNMF arrays. Figures 5(a)–(d), $l_1 = l_2$, $w_1 = w_2$, $h_1 = h_2$, and $d_1 = d_2$ are sequentially varied with fixed other parameters as in the control group. However, figures 5(e)–(h) show that the parameters of input part are varied and the parameters

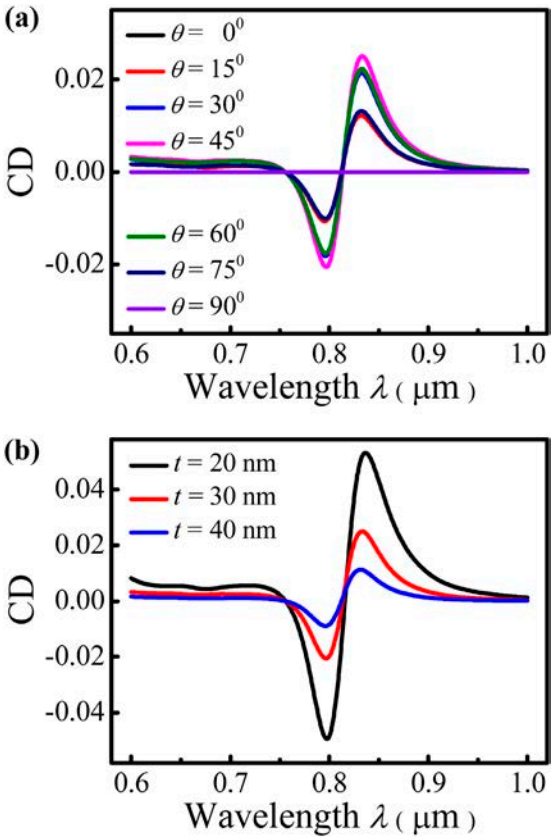

Figure 6. CD spectra of TNMF arrays with (a) different θ values and (b) different t values.

of output part are fixed as in the control group. As shown in figures 5(a) and (e), direct and indirect coupling modes red shift with increased nanorod length because of increased $\lambda_{LC-\text{in}}$ or $\lambda_{LC-\text{out}}$ with increased nanorod length, as shown in equations (3) and (4). Similarly, figures 5(b)–(d) and (f)–(h) show direct and indirect coupling mode blue shift with because of $\lambda_{LC-\text{in}}$ or $\lambda_{LC-\text{out}}$ with increased w, h, or d of nanorods in equations (3) and (4). Figures 5(a)–(d) show that the impedances of input and output parts always match because of the identical parameters in the input and output parts, which induces monotonic variations in the CD magnitudes of indirect coupling modes. However, only when $l_1 = l_2$, $w_1 = w_2$, $h_1 = h_2$, and $d_1 = d_2$ does $Z_{\text{in}} = Z_{\text{out}}$, as shown in figures 5(e)–(h). Consequently, the magnitudes of indirect coupling mode reach their maximum. In figures 5(a)–(h), the magnitudes of direct coupling mode always monotonically vary with the monotonical variation in geometric parameters. This result is due to the fact that the gold layer does hardly change in the coupling between the two nanrods. Then, the direct coupling mode cannot be explained by impedance matching.

In addition, we investigate the effects of rotary angle θ between two nanorods and the thickness of middle gold layer on the CD spectra of TNMF arrays. Figure 6(a) shows the CD spectra of TNMF arrays with increased θ from 0° to 90°. Given that TNMF arrays are achiral when $\theta = 0°$ or $\theta = 90°$, the value of black and violet lines is zero, as shown in figure 6(a). Figure 6(b) shows the CD spectra of TNMF arrays with increased t from 20 nm to 30 nm. Considering that the values of $\lambda_{LC-\text{in}}$ and $\lambda_{LC-\text{out}}$ do not change with changes in θ and t according to equations (3) and (4), direct and indirect coupling modes do not shift obviously. This property can aid in overcoming the deviation of θ and t in the experimental preparation. As shown in figure 6(a), when $\theta = 45°$, the magnitudes of CD signal for direct and indirect coupling modes reach their maximum because of the maximum asymmetry of the structure. Figure 6(b) shows that the magnitudes of CD signal for direct and indirect coupling modes dramatically increase with decreased t.

4. Conclusion

The CD properties of TNMF arrays are studied using the finite-element method. The transmission spectra, CD spectra, and charge distributions of TNMF arrays are investigated to understand the coupling mechanism. Results show that direct and indirect coupling modes occur in the CD spectra. The CD properties of TNMF arrays strongly depend on the structural parameters. For indirect coupling mode, top and bottom nanorods form resonators and can be regarded as receivers and emitters, respectively. When impedances of receivers and emitters match, the CD signal of the indirect coupling mode reaches the maximum. These results can help elucidate the chiral plasmonic mechanism and design new optical materials. When the gold film is powered on, the combined application between photons and electrons can be promoted.

Acknowledgments

This work was supported by National Natural Foundation of China (Grant No. 61575117), Fundamental Research Funds for the Central Universities of Ministry of Education of China (Grant No. GK201601008) and Foundation for Excellent PhD Dissertation of Shaanxi Normal University (No. X2014YB08).

References

[1] Sherman G M 1969 Circular dichroism of long wavelength forms of chlorophyll a *Nature* **224** 1108–10
[2] Kelly S M, Jess T J and Price N C 2005 How to study proteins by circular dichroism *Biochim. Biophys. Acta* **1751** 119–39
[3] Kaschke J, Gansel J K and Wegener M 2012 On metamaterial circular polarizers based on metal N-helices *Opt. Express* **20** 26012–20
[4] He Y, Larsen G K, Ingram W and Zhao Y Y 2014 Tunable three-dimensional helically stacked plasmonic layers on nanosphere monolayers *Nano Lett.* **14** 1976–81
[5] Hentschel M, Wu L, Schäferling M, Bai P, Li E P and Giessen H 2012 Optical properties of chiral three-dimensional plasmonic oligomers at the onset of charge-transfer plasmons *ACS Nano* **6** 10355–65
[6] Swasey S M, Karimova N, Aikens C M, Schultz D E, Simon A J and Gwinn E G 2014 Chiral electronic transitions in fluorescent silver clusters stabilized by DNA *ACS Nano* **8** 6883–92
[7] Slocik J M, Govorov A O and Naik R R 2011 Plasmonic circular dichroism of peptide-functionalized gold nanoparticles *Nano Lett.* **11** 701–5

[8] Ma W, Kuang H, Xu L, Ding L, Xu C, Wang L and Kotov N A 2013 Attomolar DNA detection with chiral nanorod assemblies *Nat. Commun.* **4** 2689
[9] Hendry E, Carpy T, Johnston J, Popland M, Mikhaylovskiy R V, Lapthorn A J and Kadodwala M 2010 Ultrasensitive detection and characterization of biomolecules using superchiral fields *Nat. Nanotechnol.* **5** 783–7
[10] Mochida Y, Cabral H, Miura Y, Albertini F, Fukushima S, Osada K and Kataoka K 2014 Bundled assembly of helical nanostructures in polymeric micelles loaded with platinum drugs enhancing therapeutic efficiency against pancreatic tumor *ACS Nano* **8** 6724–38
[11] Zhu Y, Xu L, Ma W, Xu Z, Kuang H, Wang L and Xu C 2012 A one-step homogeneous plasmonic circular dichroism detection of aqueous mercury ions using nucleic acid functionalized gold nanorods *Chem. Commun.* **48** 11889–91
[12] Zhu F, Li X, Li Y, Yan M and Liu S 2014 Enantioselective circular dichroism sensing of cysteine and glutathione with gold nanorods *Anal. Chem.* **87** 357–61
[13] Maoz B M, van der Weegen R, Fan Z, Govorov A O, Ellestad G, Berova N and Markovich G 2012 Plasmonic chiroptical response of silver nanoparticles interacting with chiral supramolecular assemblies *J. Am. Chem. Soc.* **134** 17807–13
[14] Gansel J K, Thiel M, Rill M S, Decker M, Bade K, Saile V and Wegener M 2009 Gold helix photonic metamaterial as broadband circular polarizer *Science* **325** 1513–5
[15] Wang B, Zhou J, Koschny T and Soukoulis C M 2009 Nonplanar chiral metamaterials with negative index *Appl. Phys. Lett.* **94** 151112
[16] Pendry J B 2004 A chiral route to negative refraction *Science* **306** 1353–5
[17] Plum E, Zhou J, Dong J, Fedotov V A, Koschny T, Soukoulis C M and Zheludev N I 2009 Metamaterial with negative index due to chirality *Phys. Rev.* B **79** 035407
[18] Gansel J K, Latzel M, Frolich A, Kaschke J, Thiel M and Wegener M 2012 Tapered gold-helix metamaterials as improved circular polarizers *Appl. Phys. Lett.* **100** 101109
[19] Zhang Z Y and Zhao Y P 2007 Optical properties of helical Ag nanostructures calculated by discrete dipole approximation method *Appl. Phys. Lett.* **90** 221501
[20] Esposito M, Tasco V, Todisco F, Benedetti A, Tarantini I, Cuscunà M and Passaseo A 2015 Tailoring chiro-optical effects by helical nanowire arrangement *Nanoscale* **7** 18081–8
[21] Wang Y K, Deng J C, Wang G, Fu T, Qu Y and Zhang Z Y 2016 Plasmonic chirality of L-shaped nanostructure composed of two slices with different thickness *Opt. Express* **24** 2307–17
[22] Cao T, Zhang L, Simpson R E, Wei C and Cryan M J 2013 Strongly tunable circular dichroism in gammadion chiral phase-change metamaterials *Opt. Express* **21** 27841–51
[23] Decker M, Klein M W, Wegener M and Linden S 2007 Circular dichroism of planar chiral magnetic metamaterials *Opt. Lett.* **32** 856–8
[24] Singh R, Plum E, Menzel C, Rockstuhl C, Azad A K, Cheville R A, Lederer F, Zhang W and Zheludev N I 2009 Terahertz metamaterial with asymmetric transmission *Phys. Rev.* B **80** 153104
[25] Wang Y K, Wen X J, Qu Y, Wang L, Wan R G and Zhang Z Y 2016 Co-occurrence of circular dichroism and asymmetric transmission in twist nanoslit-nanorod arrays *Opt. Express* **24** 16425–33
[26] Decker M, Ruther M, Kriegler C E, Zhou J, Soukoulis C M, Linden S and Wegener M 2009 Strong optical activity from twisted-cross photonic metamaterials *Opt. Lett.* **34** 2501–3
[27] Yin X, Schäferling M, Metzger B and Giessen H 2013 Interpreting chiral nanophotonic spectra: the plasmonic Born–Kuhn model *Nano Lett.* **13** 6238–43
[28] PingáYeo S 2013 Theoretical realization of robust broadband transparency in ultrathin seamless nanostructures by dual blackbodies for near infrared light *Nanoscale* **5** 3373–9
[29] Qu Y, Tian X, Fu T, Wang G, Li G and Zhang Z 2015 Broadband extraordinary optical transmission through a multilayer structure with a periodic nanoslit array *IEEE Photonics J.* **7** 1–8
[30] Johnson P B and Christy R W 1972 Optical constants of the noble metals *Phys. Rev.* B **6** 4370
[31] Hao J, Qiu C W, Qiu M and Zouhdi S 2012 Design of an ultrathin broadband transparent and high-conductive screen using plasmonic nanostructures *Opt. Lett.* **37** 4955–7
[32] Tominaka T 2011 Current distribution calculation for a superconducting multi-layered power cable *Cryogenics* **51** 630–4